ORIGINAL PAPER

Soil site characterization of Rabigh city, western Saudi Arabia coastal plain, using HVSR and HVSR inversion techniques

Abdullah M. Alamri[1] · Abdalaziz Bankher[2] · Kamal Abdelrahman[1,3] · Mahmoud El-Hadidy[3] · Hani Zahran[2]

Abstract

Rabigh city located along the coastal plain of the Red Sea in western Saudi Arabia is economically significant. This pioneering study assesses the site characterization of Rabigh city based on integrated geological, geotechnical, and seismological data. These datasets include geotechnical data from 100 boreholes, 127 microtremor records, and detailed geologic maps of the area of study. The grid interval for microtremor sites is 1 km. The fundamental resonance frequency (f_o) and maximum amplification factor (A_o) are identified from the horizontal-to-vertical spectral ratio (HVSR) curves from the recorded data. The distribution map of f_o displays three distinct zones, high fundamental frequency (greater than 1 Hz), moderate (0.5 Hz– Hz), and low (less than 0.5 Hz), while the obtained A_o ranges between 2 and 4.2. The horizontal-to-vertical spectral response inversion technique has been conducted for 40 microtremor records in the frequency band 0.2–5 Hz to evaluate the shear-wave velocity for 30 m depth (Vs_{30}). The computed values of Vs_{30} range from 208.5 m/s to 516 m/s. According to the National Earthquake Hazard Reduction Program (NEHRP) soil site characterization, Rabigh city is differentiated into two soil classes, C and D. The detailed geotechnical investigations for sabkhah sediments are highly recommended for reducing their environmental risks to urban facilities and economic projects in Rabigh area.

Introduction

Rabigh city lies along the eastern Red Sea coast of western Saudi Arabia, to the north of Jeddah city (Fig. 1). This city is the major commercial and industrial center of Makkah Province, as it contains many industrial factories and facilities (e.g., petrochemical, cement, power cables, and steel). Furthermore, it is the connection between the urban areas in Jeddah and the industrial centers in Tabuk Province to the north. Therefore, it is attractive for the Saudi government

and planners to construct mega projects, which require huge infrastructure. The examination of the local ground conditions is valuable for seismic site characterization (Fäh et al. 2003). It is well-known that the soft stratigraphic layers can greatly amplify ground motion in the event of an earthquake (Farrugia et al. 2016). Furthermore, the calculation of the shear-wave velocity (V_S) and/or the resonance frequency of the soft soil layers are significant steps to predict the ground motion and prevent or mitigate of earthquake disasters (Arai and Tokimatsu 2004). These information should be oriented to earthquake-risk mitigation strategies (Zor et al. 2010).

Through the past few decades, the passive seismic techniques, such as using of the acquisition of ambient vibrations (microtremors), which are supposed to be dominated by surface waves, have been developed and are becoming increasingly popular (Farrugia et al. 2016). These procedures are useful because they provide quick and reliable estimates of subsurface soils, using relatively cheap equipment, enabling simple deployment in urban zones (Parolai et al. 2005). The horizontal-to-vertical spectral ratio (HVSR) technique represents one of the experimental methods which applied to evaluate some characteristics of soft sediments and soils
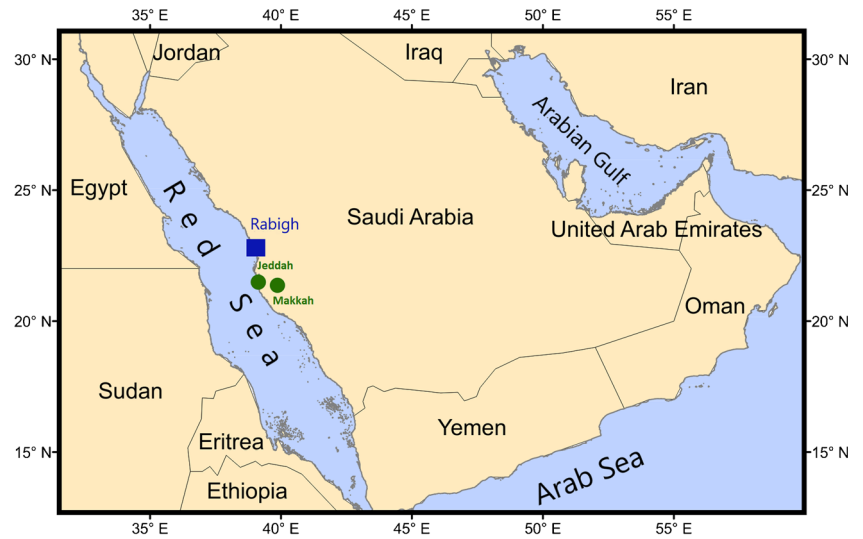
✉ Kamal Abdelrahman
khassanein@ksu.edu.sa

[1] Department of Geology & Geophysics, College of Science, King Saud University, P.O. Box 2455, Riyadh 11451, Saudi Arabia

[2] National center of earthquakes and volcanoes, Saudi Geological Survey, Jeddah, Saudi Arabia

[3] Seismology Department, National Research Institute of Astronomy and Geophysics, Cairo, Egypt

(SESAME 2004). This technique has proven to be valuable in estimating the fundamental frequency and the amplification factor of soil deposits. Through this study, microtremor data was acquired from 127 sites in Rabigh city. Also, geotechnical data was gathered from 100 boreholes. The average shear-wave velocity for the uppermost 30 m (Vs_{30}), depending on the travel time from the surface to 30 m depth, is acquired from the HVSR inversion and used in soil classification.
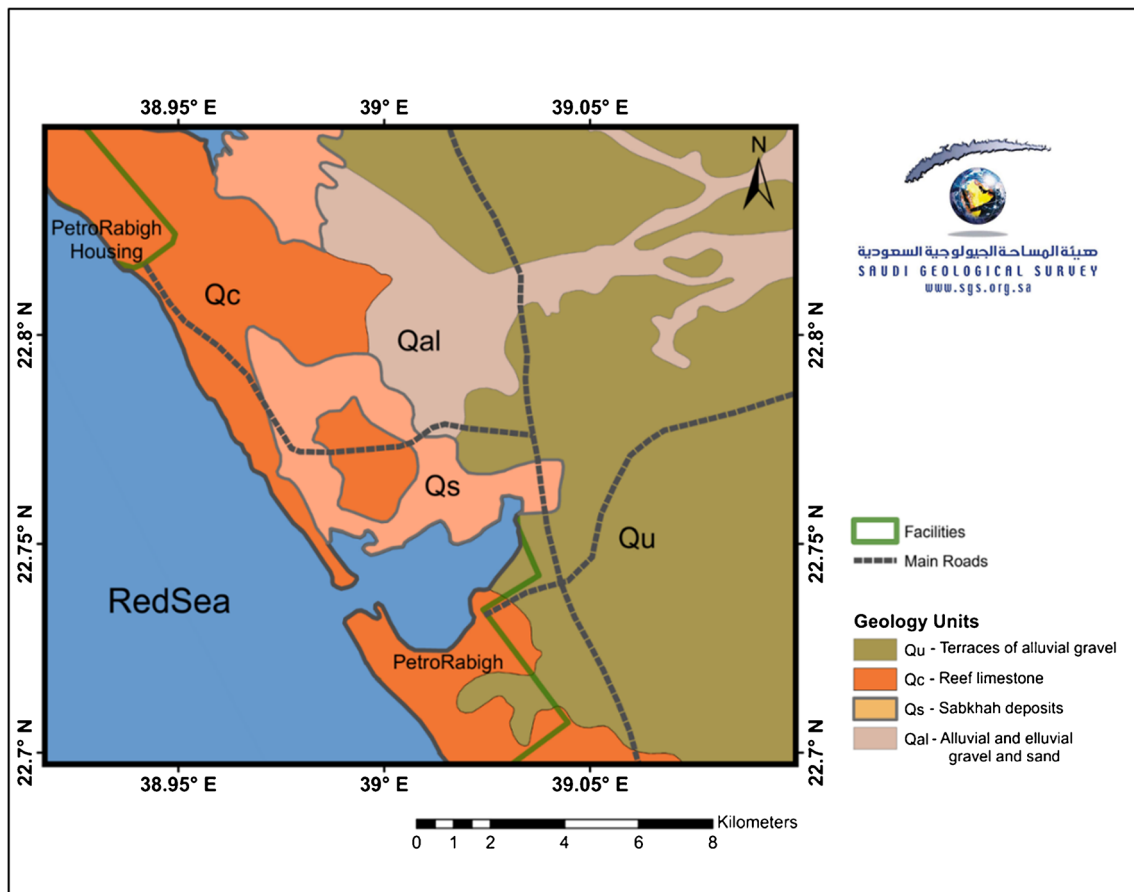
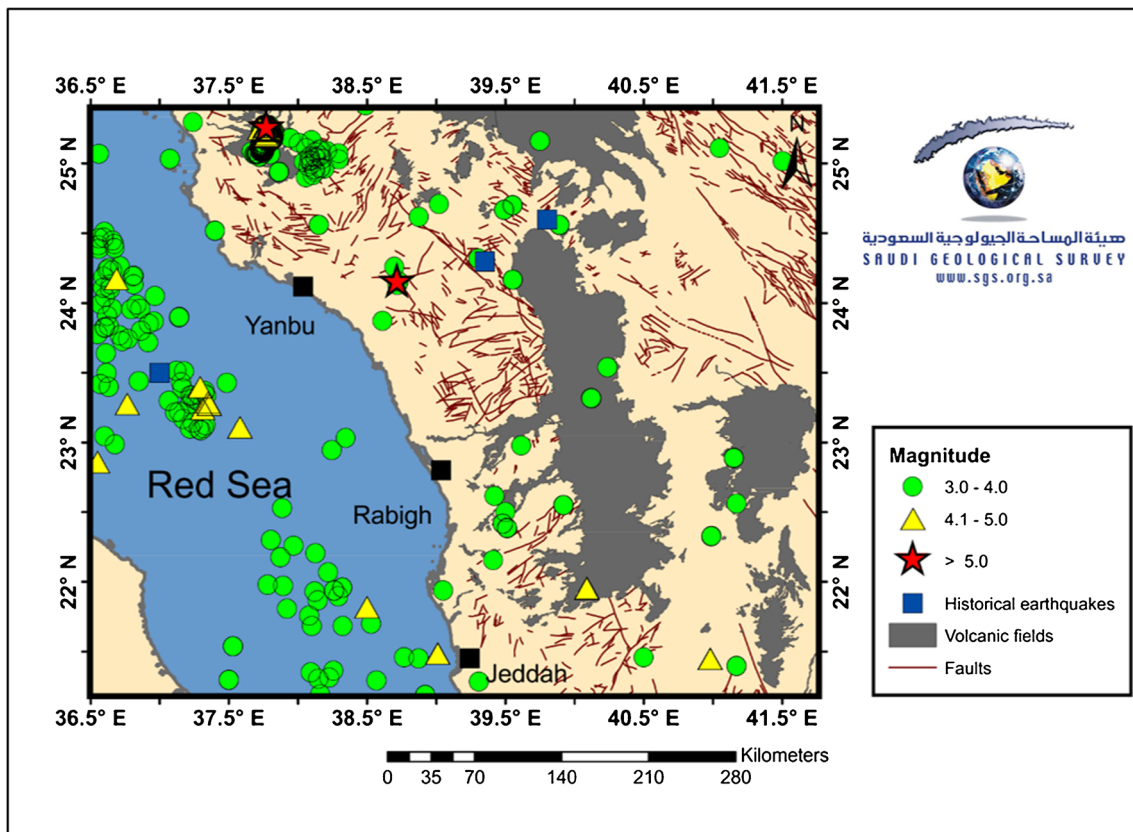**Fig. 2** Geology of Rabigh (after Ramsay 1986)

Fig. 3 The seismicity of Rabigh area (after SGS)

Local geology of Rabigh area

The outcropping rocks in Rabigh area are represented, westward, by Precambrian basement rocks overlain unconformably by Tertiary sedimentary rocks due west and by Miocene to Pliocene lavas in the northern part (Moore and Al-Rehaili 1989). Widespread areas of Quaternary surficial deposits (sand and gravel) cover the coastal plain and major wadis. Raised Quaternary coral reefs form two prominent terraces on the Rabigh area coast (Dawood et al. 2013). Ramsay (1986) subdivided these deposits into six geological units, the oldest being the reef limestone (Qc). This rock unit outcrops in a 2 to 5 km wide zone spreads parallel to the coast. In the south, the outcrop is less continuous, giving way to sabkhah

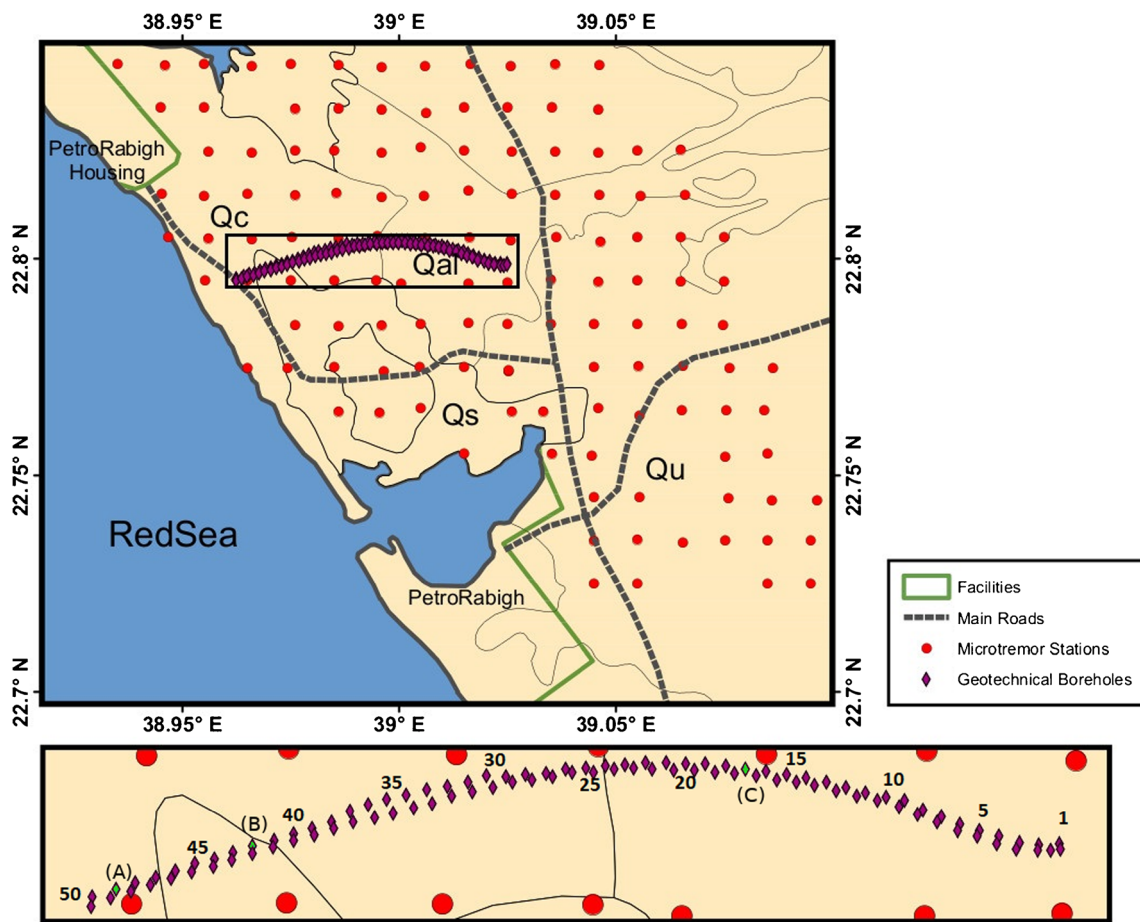**Fig. 4** Methodology flowchart applied in the present study
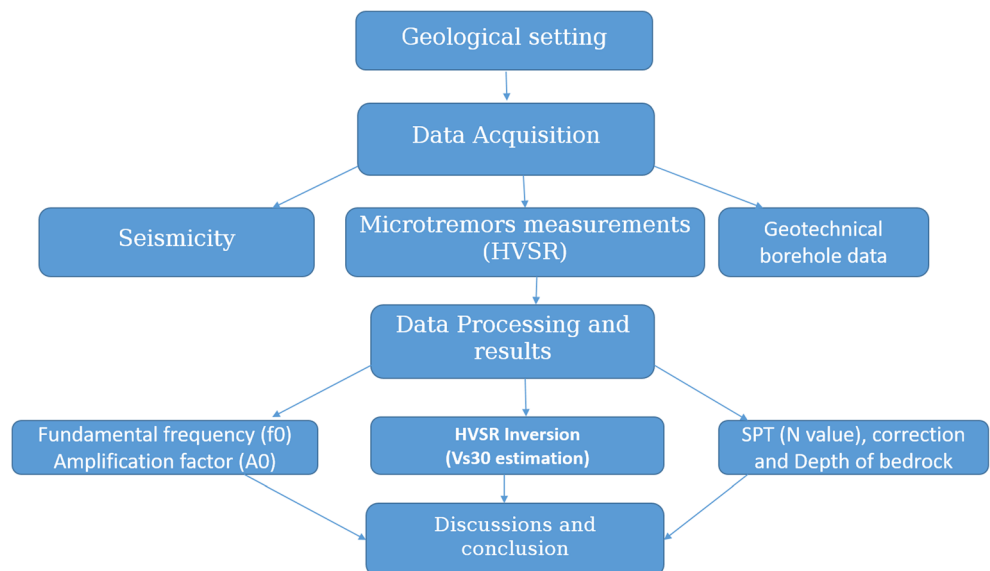
Fig. 5 Distribution of microtremor measuring sites and geotechnical boreholes in Rabigh city

deposits (Qs), and to the east, it is covered by alluvial terraces and fans (Qu) that mostly have an intricate, shallow, dendritic drainage system. The most recent deposits are alluvial and eluvial gravels and sands (Qal); the former fills the bottoms of wadis due to the weathering process of plutonic rocks. In places, windblown sand (Qe) overlies the gravel terraces and alluvial fans (Qu) with a thin veneer, banked up against rocky hills. Boulder fans of talus (Qt) develop where isolated rocky hills stand in the coastal strip or adjacent to steep hills in the mountain areas.

Rabigh city is located across four different soft deposits due to its location on the coastal plan and on the downstream of one of the major wadis in the area (Fig. 2). According to Ramsay (1986), major parts of the coastal strip are covered by terraces of alluvial gravel (Qu) that range from a thin layer to several meters thick; pediments occur inland at the foothills of mountains, and gravel terraces are accumulated in the major wadis. Well-sorted gravels, with pebbles and cobbles, mostly ranging from 5 to 10 cm, are widespread on the coastal plain, particularly on every side of the lower reaches of Wadi Rabigh. Ramsay (1986) described the reef limestone (Qc), which encountered as a discontinuous belt along the coastal zone, typically with a flat reef platform for a few hundred

meters on the seaward side. On the shoreward side, the reef limestone is elevated 2 to 4 m above mean sea level and forms flat ground, overlapped by sabkhah or terrace-gravel deposits. Wadi-generated alluvial sediments (Qal) are widespread on the coastal plain, stretching seaward from the mouths of all the major wadi systems and filling low-lying areas (Ramsay 1986). In the lower reaches of the main wadis, the alluvial sediments reach depths on the order of 15 m, and in minor tributary wadis, the alluvium is rarely more than 5 m thick. Sabkhah deposits (Qs) are several low-lying, saline mudflats that occur immediately behind the coast, comprised of brown terrigenous sands and clays (Ramsay 1986). Also, these deposits generally have a salty crust with, in minor depressions, a white layer of salt with 0.5 m thick. Sediments beneath the crust are moist and contain interstitial gypsum.

Hydrogeologically, Rabigh basin area is affected by two types of drainage networks. The tributaries emerging from the northeastern volcanic ridge of the eruptive centers are strictly controlled by the incipient flow pattern of the basaltic lava (Zaigham et al. 2017). Thus, the courses of these tributaries ran within the basalts. On the other hand, another lava flow tongue of Harrat Rahat partly has occupied the south and southeastern parts of the Rabigh basin. Several smaller northwestward bifurcations
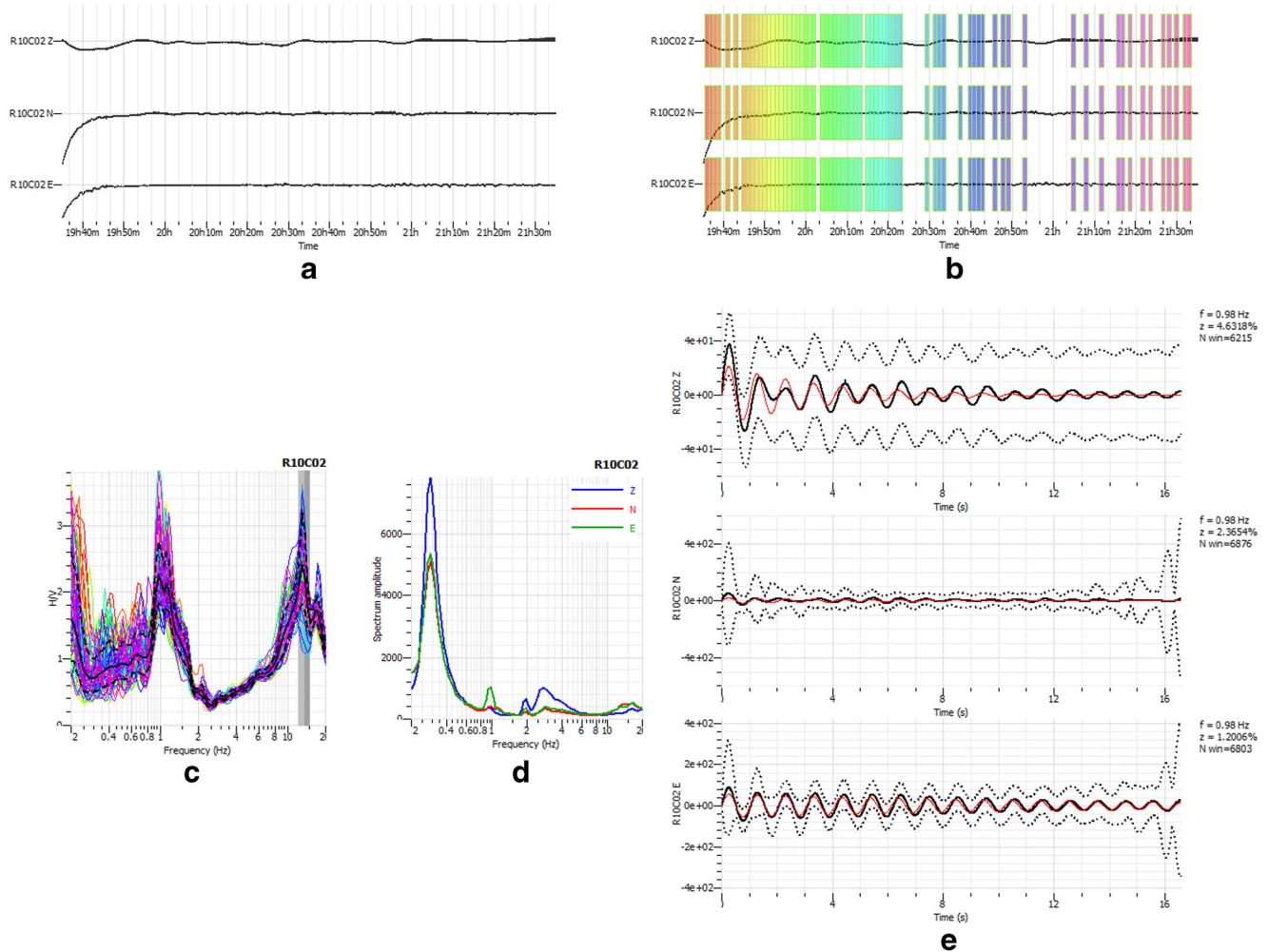
Fig. 6 Processing sequence, (**A**) time series for three components record, (**B**) selected windows in the time domain, (**C**) windows after transformed to frequency domain by fast Fourier transform (FFT), (**D**) H/V spectra, and (**E**) damping test

of this basaltic lava flow tongue were found intruded into the fault/fracture zones prevailing within the Precambrian rock units. All these fault/fracture zones were also observed serving as the passage for the courses of the tributaries passing across the exposed Precambrian terrain forming a complex drainage network in the area associated with the main wadi Rabigh.

The drainage pattern in the downstream areas does not apparently show the distinct distributaries of the wadi Rabigh in coastal flood plain region. The development of tributaries is continuous even in the downstream portion of the basin from the relatively low elevated but steeper hilly mountainous front. This trend indicates steep gradient along the coastline areas, which in turn, shows the possibility of Holocene up-rising.

Seismicity of the Rabigh area

The seismicity of Rabigh city and its surrounding areas was obtained from Ambraseys et al. 1994, the International Seismological Center (ISC), the Saudi National Seismic Network (SNSN), King Saud University (KSU), the King Abdulaziz City for Science and Technology (KACST), and the Saudi Geological Survey (SGS), as presented in Fig. 3. The Red Sea earthquakes are concentrated along the main axial trough (Almadani et al. 2015). The location of earthquakes in the western part of the Arabian Shield is related to seafloor spreading and volcanism in the Red Sea (Zahran et al. 2016). Significant historical earthquakes (Fig. 3), these are the 1121 AD magnitude 6.8 M_F earthquake from the main Red Sea trough (latitude 23.5° N, longitude 37° E) (Ambraseys et al. 1994), and the 30 January 1256 AD in the Hejaz region, about 132 km east of Yanbu. Recently, seismic instrumentation recorded significant earthquakes, including a M_w 3.7 event that occurred on 27 August 2009 (38.75 N, 24.13 E) about 68 km east of Yanbu city (Aldamegh et al. 2012). Zahran and El-Hady (2017) stated that an earthquake swarm, of over 15,000 events, occurred in Harrat Lunayyir, with a maximum magnitude of M_w 5.7 on 19 May 2009. This earthquake swarm was caused by magmatic dike intrusion.
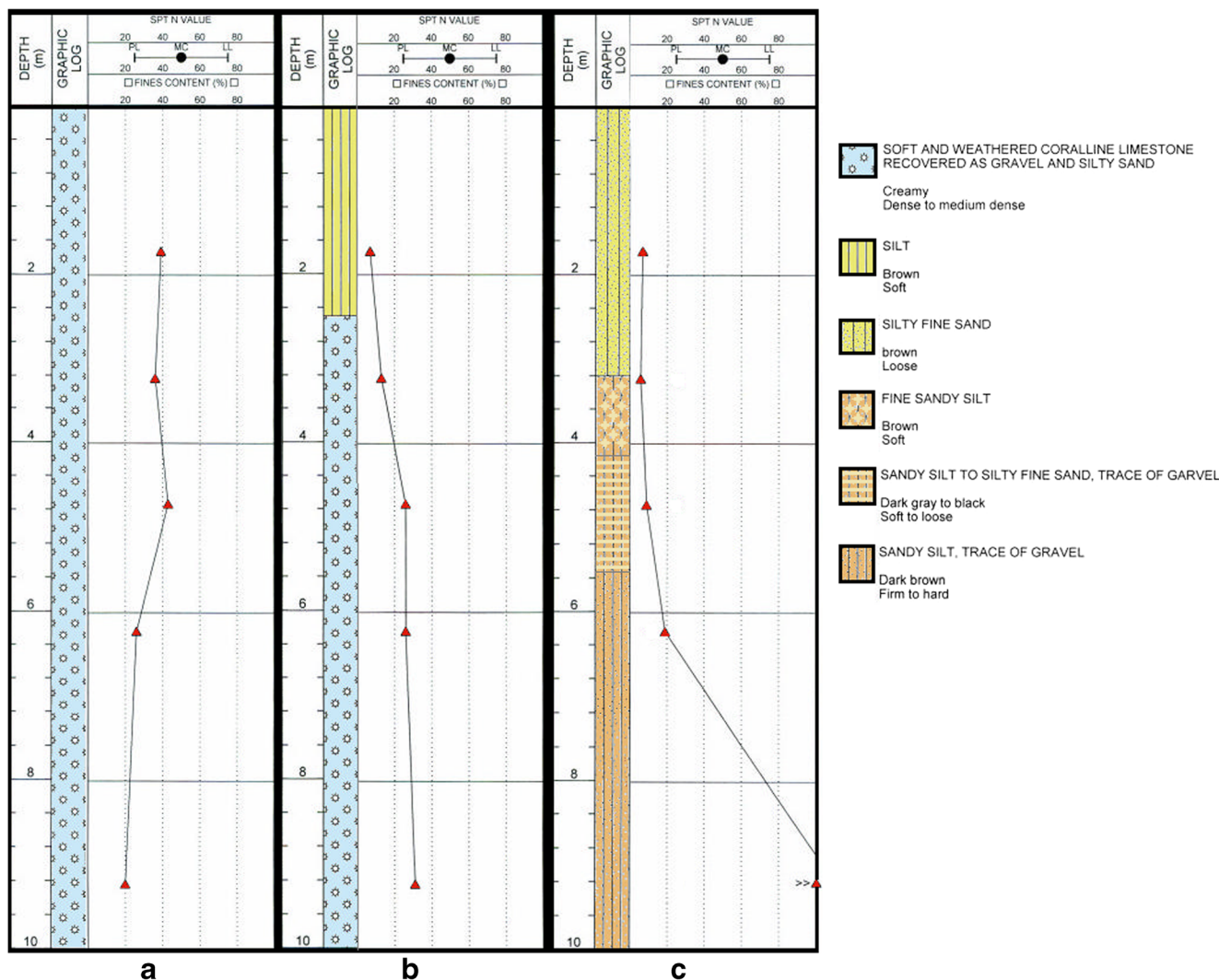
Fig. 7 Boreholes data in three geological units, (**A**) coralline limestone, (**B**) sabkhah, and (**C**) alluvial and elluvial deposit (after Adel Engineering Office)

Methodology

There are different types of data collected throughout this study including microtremor measurements (HVSR), geotechnical borehole data, and HVSR inversion to estimate Vs$_{30}$ parameter. These integrated data were treated according to flowchart in Fig. 4. The HVSR technique offers the dynamic features for ground and structures to be gathered (Nakamura 1989) based on microtremors measurements. When the soil layer is exposed by the ambient noise, the soil transfer function can be assessed depending on Eq. (1):

$$S_T = \frac{H_s(f)}{H_B(f)} \tag{1}$$

where H$_S$ and H$_B$ are the spectral amplitudes of the horizontal components of microtremors acquired at the surface of the soil layer and at bedrock level respectively. This transfer function peaks up at the fundamental resonance frequency of the soil. The source effect has to be removed before defining the impact of the soil. The H/V spectral curves suppose the source spectrum, Ss, can be assessed using Eq. (2) as follows:

$$S_S = \frac{V_S(f)}{V_B(f)} \tag{2}$$

where V$_S$ and V$_B$ are the spectral amplitudes of the vertical components computed at the surface of the soil layer and at the bedrock level respectively. Dividing Eq. (1) by (2) offers the soil transfer function, assuming that H$_B$/V$_B$ = 1, as follows:

$$HVSR(f) = \frac{S_T}{S_S} = \frac{H_S}{H_B} \cdot \frac{V_B}{V_S} = \frac{H_S}{V_S} \tag{3}$$

As a result, the transfer function (HVSR) of a site can be evaluated according to the spectral ratio of the horizontal and vertical components acquired for selected site (Nakamura 1989; Delgado et al. 2000; Mendecki et al. 2014). HVSR computations are obtained using the Geopsy software

Fig. 8 HVSR inversion sites
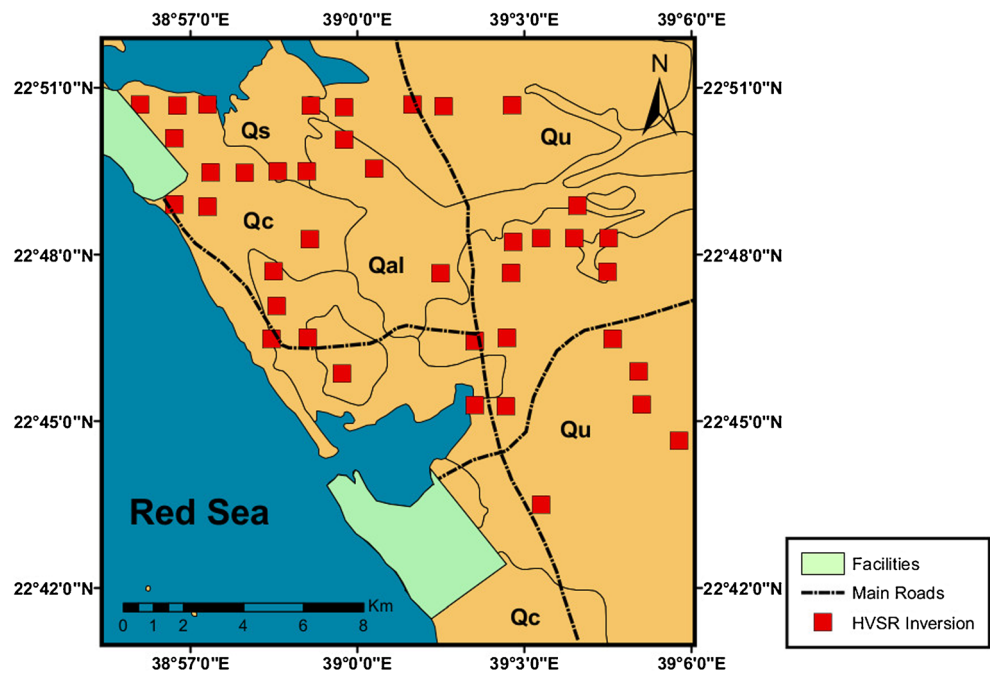
(Wathelet 2006) which was designed under the SESAME European research project WP12 (2004). Short-duration instabilities of the signal were avoided during H/V processing through anti-trigger window selection to remove transient signals. The used window length is 60 s. The current analysis was conducted to the frequency range from 0.2 Hz to 20 Hz. The time series was tapered with a cosine taper, and the amplitude spectrum has been identified for every component.

The FFT spectra were smoothed using the algorithm of Konno and Ohmachi (1998). The two horizontal components were merged using the squared average methodology. The H/V for each time window was calculated, then an average H/V curve was calculated. The reliability of the produced H/V curves and peaks was examined using the criteria of the SESAME project (2004). Aldahri et al. (2018) followed the same processing scheme at Ubhur district in Jeddah using HVSR.

Fig. 9 The distribution of fundamental frequency (f_o) in Rabigh city
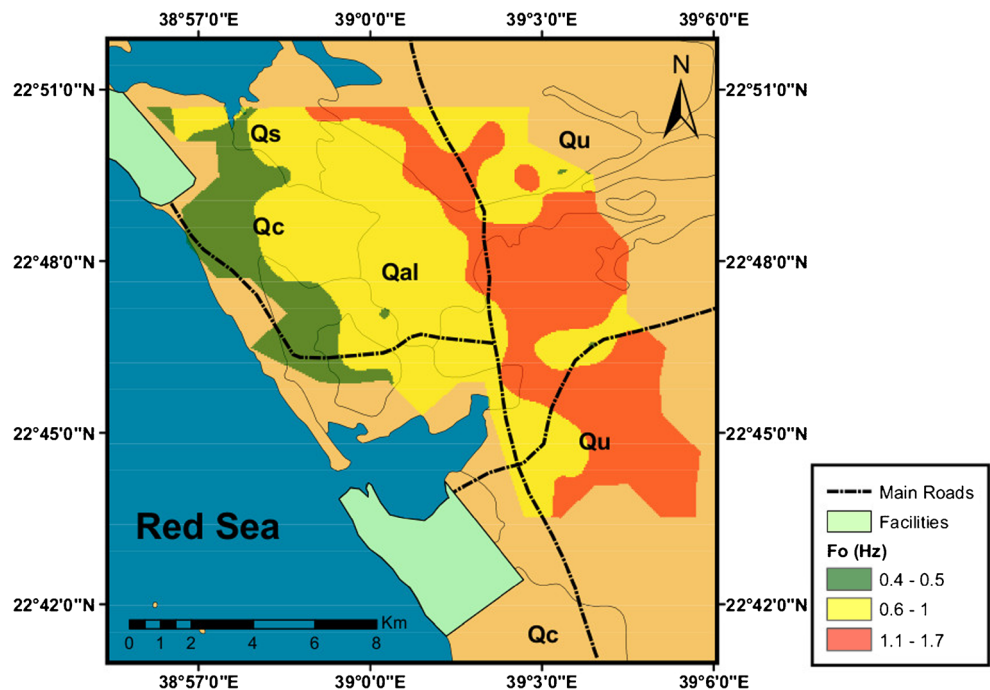
Fig. 10 The maximum amplification factor (A_o) distribution map of Rabigh city
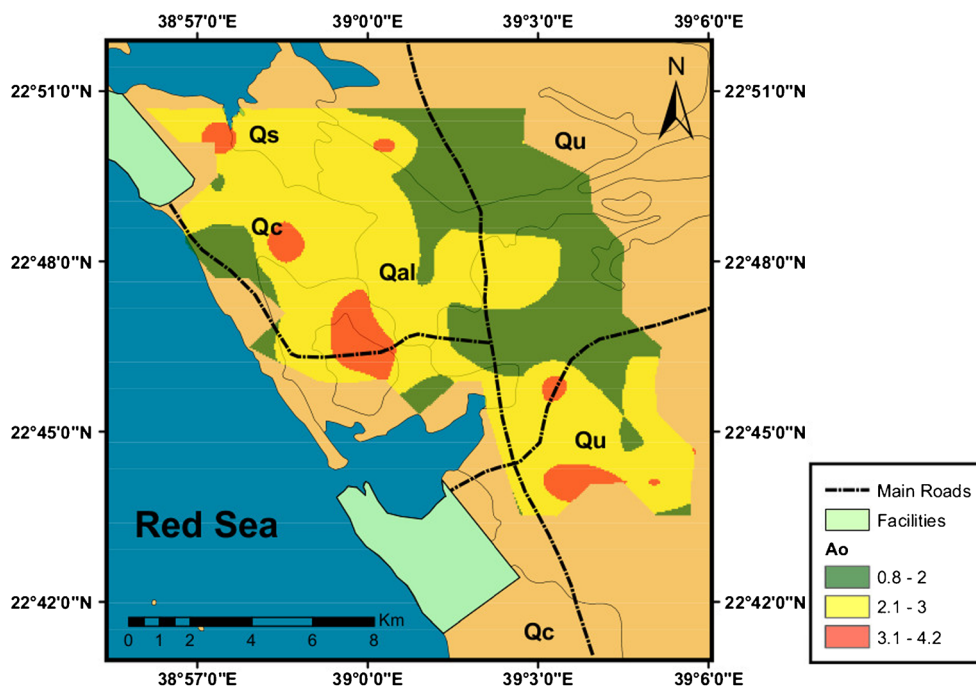
The inversion modeling process carried out depending on HVSR curves that calculated using third-party software (e.g., Grilla, Geopsy, etc.). The forward modeling routine (FWD) estimates the theoretical transfer function of a subsurface layers following the approach of Tsai and Housner (1970). They supposed that the subsurface structure composed of viscoelastic homogeneous layers overlaying half-space in terms of thickness (H), density (ρ), primary and shear-wave velocities (Vp, Vs), and their attenuation factors (Qp, Qs) that are frequency dependent and are calculated by the following equation:

$$Q = Q_0 f^k \tag{4}$$

where Q_0 is the attenuation factor at 1 Hz and k is a constant. Finally, the dispersion of body waves is measured using Aki and Richards (2002) logarithmic law;

$$v(f) = v\left(f_{ref}\right)\left[1 + (\pi Q_0)^{-1}\ln\left(f/f_{ref}\right)\right] \tag{5}$$

The estimated 1D subsurface model for every site has been conducted through the FWD to compute the amplification spectra of body waves. But at the same time, surface waves cannot be ignored because of both body and surface waves can affect the experimental HVSR curves (Nakamura 1996, 2000). So, the role of surface waves can be simulated using the modeling approach of Lunedei and Albarello (2010). The relationship between HVSR and the S-wave transfer function has to be identified depending on the major effect of body waves of HVSR maxima (Bard 1999; Nakamura 2009), then the relation between the HVSR function and S-wave response function is expected (Nakamura 2000, 2009; Herak 2008).

The inferred theoretical HVSR curves, within the generalized surface wave suggestion (Lunedei and Albarello 2009), were used to check the role of surface wave in the computed HVSR curves where the propagated surface waves with multimodal velocities were considered. So, the expected HVSR curves have been estimated as a function of Vs, Vp, density, and damping according to Lunedei and Albarello (2009) approach:

$$HVSR(\omega) = \sqrt{\frac{P_H(\omega)}{P_Z(\omega)}} \tag{6}$$

where

$$P_H(\omega) = \sqrt{P_r(\omega) \cdot P_\vartheta(\omega)} \tag{7}$$

The inversion process followed Monte Carlo (MC) method to simulate the best fitted HVSR curves depending on material parameters which varies with depth. The input different groups of parameters (Vp, Vs, H, Qp, Qs) yield different shapes of the theoretical HVSR curves. Consequently, the simulated curves with best correlation with the HVSR curves inferred from the experimental data will be selected where the peaks in the HVSR curve is considered as the main criterion for selection, while the width and amplitude of the peaks will provide considerable information for subsurface impedance contrasts.
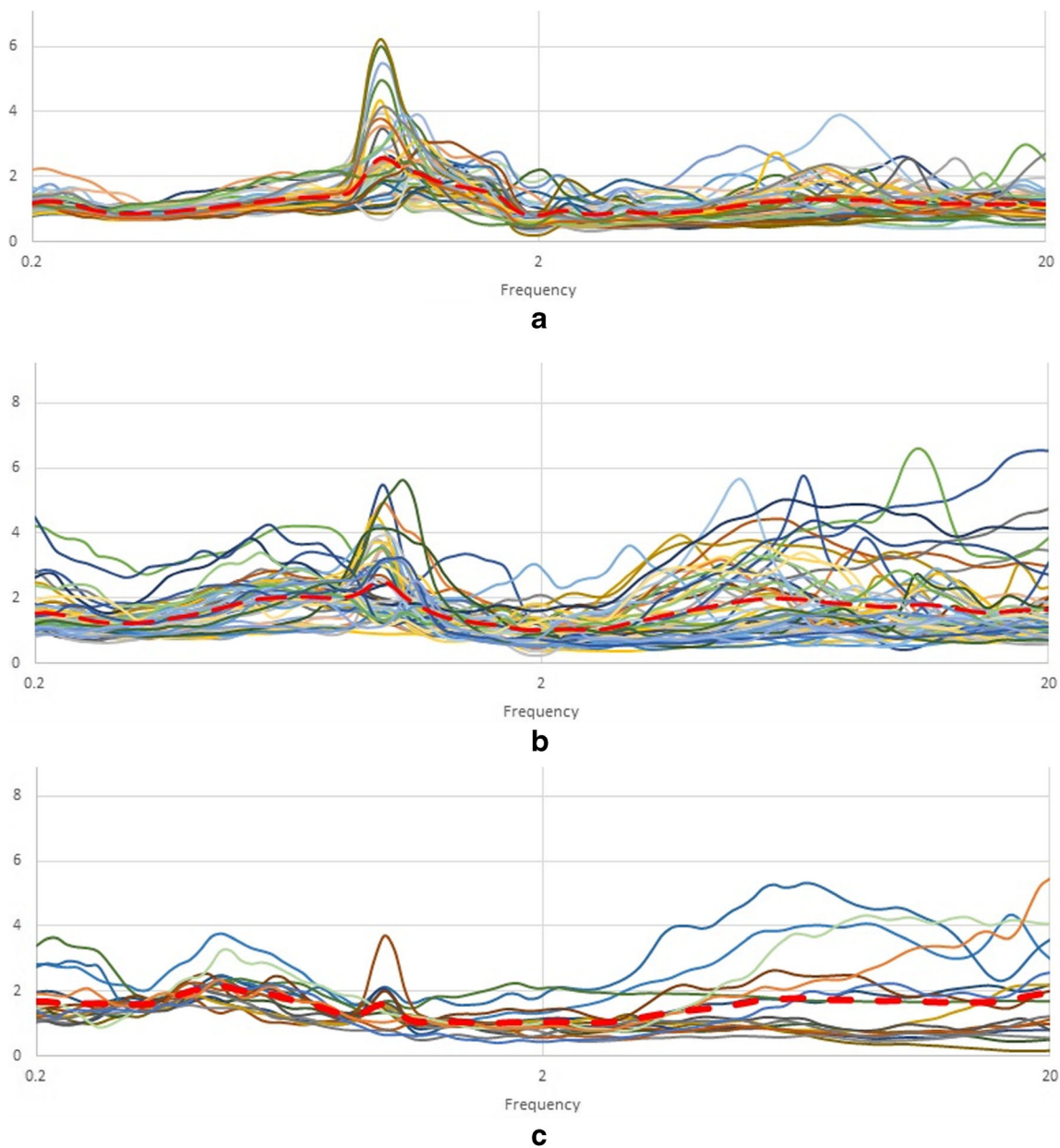
Fig. 11 The HVSR curves in the high f_o zone (**A**), moderate f_o (**B**), and low f_o zone (**C**), where the red line represents the average HVSR curve in each zone

Data collection and processing

Microtremors field measurements

Microtremors data were collected for 127 measuring sites covering the whole area of Rabigh city (Fig. 5) where all area has been divided into grid of profiles with area of 1 km². In urban areas, the data were acquired at night, while data from other sites were collected at early morning. The recording station includes a three-component seismometer (Trillium compact 120), synchronized global positioning system (GPS), and handheld Taurus portable data acquisition unit with excellent data quality of 24-bit resolution. The frequency sampling rate was 100 sample per second. The recording length extends from 90 and 270 min for every site, while the stations interval was approximately 1 km. The quality of the acquired data was checked consciously during field measurements at every site to select high quality data. The guidelines of the SESAME project have been considered to ensure reliable experimental conditions. Figure 6 illustrates the used H/V data process scheme.

Geotechnical borehole data acquisition

The available geotechnical boreholes are extending in a line following the path of the main highway road through the city

Table 1   Shear velocity model from HVSR inversion

Site ID	Layer 1		Layer 2		Layer 3		Layer 4	
	Vs	H	Vs	H	Vs	H	Vs	H
1	256.64	3.41	546.06	12.47	459.20	44.08	922.73	999
2	271.80	3.75	473.50	16.47	448.22	61.21	747.66	999
3	313.35	2.24	522.22	14.84	391.48	41.36	780.10	999
4	209.19	4.04	342.25	14.66	401.09	62.34	861.54	999
5	139.86	3.10	237.55	15.26	300.86	38.50	804.28	999
6	197.30	3.51	451.27	12.03	454.31	54.75	825.47	999
7	193.21	2.43	431.01	10.22	626.20	49.19	839.88	999
8	121.40	3.38	159.76	9.27	381.70	44.25	716.18	999
9	171.01	5.24	289.79	8.85	282.42	43.94	802.08	999
10	271.67	3.11	168.40	14.59	345.96	37.80	679.53	999
11	164.06	5.51	290.32	7.35	260.81	48.81	670.29	999
12	122.75	2.33	503.99	9.13	574.65	15.63	1103.58	999
13	189.17	2.79	365.72	8.81	412.77	60.04	832.38	999
14	176.79	3.12	274.50	9.63	447.86	58.84	777.99	999
15	230.42	2.96	502.69	10.66	483.43	49.65	819.13	999
16	230.85	5.80	327.91	8.38	379.02	49.69	737.85	999
17	183.93	4.26	194.24	9.77	294.84	34.89	654.61	999
18	119.26	4.85	167.36	8.38	249.96	42.58	549.86	999
19	178.46	4.01	369.48	14.03	471.56	64.86	944.13	999
20	207.57	4.64	328.06	19.96	516.98	48.46	700.65	999
21	175.60	3.50	250.51	13.55	459.09	63.52	821.12	999
22	240.15	3.90	229.54	15.26	420.59	43.43	808.66	999
23	169.59	2.69	487.49	12.99	461.25	27.49	825.47	999
24	305.63	4.30	253.33	16.01	474.40	48.37	670.27	999
25	201.48	4.91	251.31	16.21	450.78	46.72	831.78	999
26	158.48	6.61	215.72	12.14	331.87	51.08	614.50	999
27	251.12	3.34	314.08	12.74	462.54	48.84	903.09	999
28	246.90	3.08	387.98	12.95	396.58	63.26	795.52	999
29	304.19	3.71	255.91	17.56	495.77	52.12	918.52	999
30	205.00	3.47	303.86	21.63	391.88	49.60	639.93	999
31	197.62	3.59	286.04	16.40	302.31	54.23	709.54	999
32	253.84	3.18	453.24	13.00	449.27	51.72	825.47	999
33	229.42	2.89	316.35	6.50	605.48	41.28	704.82	999
34	223.42	3.31	344.28	19.85	417.48	45.00	1307.97	999
35	211.82	2.23	417.21	6.39	558.34	45.23	825.47	999
36	220.21	2.62	560.76	17.67	396.17	59.66	1374.59	999
37	273.01	3.48	318.40	19.84	357.67	63.26	850.14	999
38	167.49	4.12	305.19	20.63	440.76	66.08	962.34	999
39	244.29	3.15	413.14	19.07	343.70	42.82	1078.73	999
40	238.93	4.67	308.93	22.84	375.01	54.75	915.46	999

including more than 100 boreholes provided by Adel Engineering Office. These boreholes cover three different geological units (Qc, Qs, and Qal) and extend down to 10 m depth (Fig. 7). Figure 7 presents three examples of borehole geotechnical data in the area of interest. Borehole

A is composed of creamy, loose to moderately dense, weathered coral limestone, while borehole B consists of sabkhah deposits forming the first layer is brown soft silt with a thickness of 2.6 m, while the second layer consti- tuted by the creamy-colored loose to moderately dense weathered coral limestone with a thickness of 7.4 m. Borehole C contains four soft soil layers as follows: the upper layer is brown, loose, silty, fine sand, 3.2 m thick; the second layer is sandy silt with a thickness of 6.8 m. This layer has a density gradient, whereby the first 1 m is brown, soft, fine, sandy silt; the third layer has 1.2 m of dark gray to black sandy silt to silty sand with a trace of gravel; and the fourth layer is comprised of 4.1 m of dark brown, firm to hard, sandy silt with a trace of gravel.

Due to the available geotechnical parameters, borehole A has SPT values in the reef limestone reaches 38 at a depth of 1.8 m. This value increased up to 43 at a depth of 4.25 m, then decreased again to 19 at 9 m depth. While, in borehole B, the SPT is 7 at a depth of 1.8 m in the silt layer, which then increased to 31 at 9 m depth. The SPT values in borehole C remain almost constant (7, 6, and 9) until 6.25 m depth, then sharply increased up to 80 at 9 m depth.

N values measured in the field using the SPT procedure have been corrected (N_{60}) for different parameters such as overburden pressure (C_N), hammer energy (C_E), borehole di- ameter (C_B), presence or absence of liner (C_S), rod length (C_R), and fines content (C_{fines}), according to the following equation (Anbazhagan and Sitharam 2008):

$$N_{60} = N \times \left(C_N \times C_E \times C_B \times C_S \times C_R \times C_{fines} \right. \quad (8)$$

These SPT values are then corrected to estimate the Vs ac- cording to Hasancebi and Ulusay (2007) using Eq. (9), which is valid for all soil in Quaternary deposits; however, Vs correlation equations are assumed depending on both N and N_{60}.
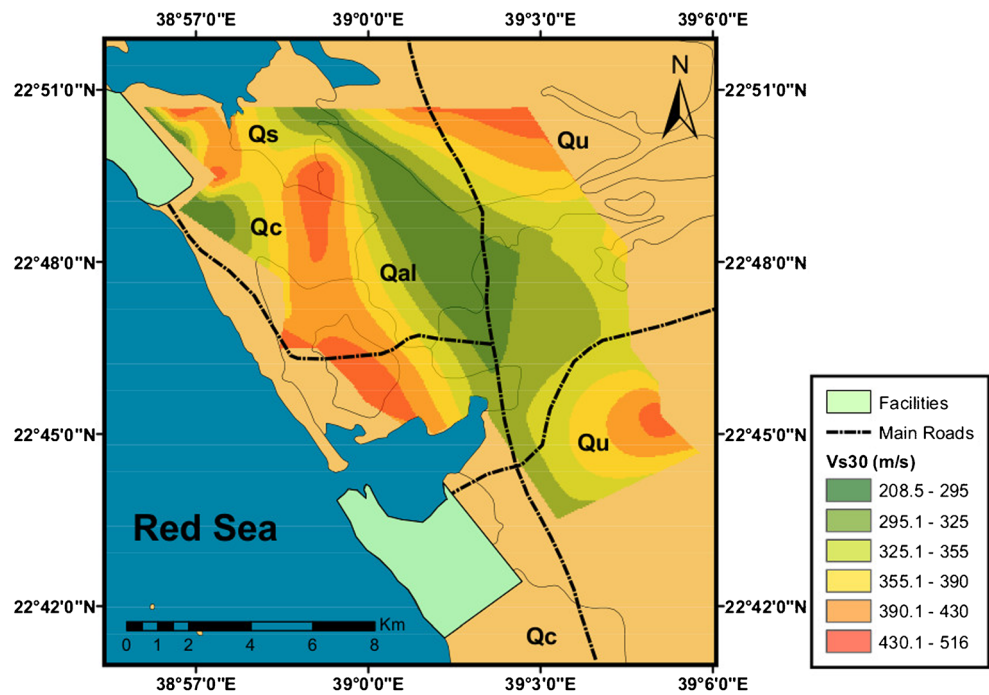
$$V_S = 104.79 N_{60}^{0.26} \quad (9)$$

The estimated Vs profile provides the initial model for HVSR inversion where the Vs for the reef limestone unit (borehole A) ranges between 225.3–278.8 m/s, while for the sabkhah (bore- hole B), the Vs values are 173.8 m/s in the first layer, varies between 204.2–255.9 m/s for the second layer. Borehole C has Vs values up to 173.8 m/s in the first layer; the second layer of borehole C, the Vs varies between 167 and 185.5 m/s for soft to loose soil, and 225.3 to 347 m/s for the firm to hard soil deposits.

HVSR inversion

HVSR inversion was applied using the OpenHVSR software (Aldahri et al, 2017; Bignardi et al. 2016; Mantovani et al.

Fig. 12 Vs_{30} distribution map in Rabigh city

Results

The obtained fundamental frequencies from the analyzed 127 microtremor record ranges between 0.41 Hz and 1.68 Hz as exposed in Fig. 9, while the corresponding A_o varies from 2 to 4.2 (Fig. 10). Based on f_o values, Rabigh area can be differentiated into three zones: 1 Hz < f_o < 1.68 Hz covering the eastern zone Rabigh area; 0.5 Hz < f_o < 1 Hz constituted the central part; and 0.41 Hz < f_o < 0.5 Hz appears as a strip in the western zone of the city. The eastern zone is distinguished by higher f_o values (1 Hz–1.68 Hz), except the northeastern sector, which has lower f_o values (0.5 Hz–1 Hz) following the path of the valley that crossing this zone. This zone is covered by Qu, except for the lower part, which, as previously mentioned, is covered by Q_{al}. The distribution of A_o in this zone is small suggesting a thin sedimentary layer (Fig. 11a). The middle zone of the city has a moderate f_o values (0.5 Hz–1 Hz) where it is overlaid by all geological units (Qu, Qs, Qc, and

Qal). It has A_o values below 4, and the highest values are appeared with the sabkhah units. In this zone, the sedimentary cover is greater than the eastern zone due to presence of the soft deposits in the valley basin (Fig. 11b). The western zone has a low f_o area (0.41 Hz–0.5 Hz) and covered by Qc and Qs, while the A_o values are less than 4 and decreased less than 2 in the southwestern corner of this zone. Based on the geological map, this zone is covered by the reef limestone layer. This area has the greatest sedimentary thickness because of the deposition along the coast (Fig. 11c).

The obtained shear velocity models through HVSR inversion and due to the representative soil profiles of Rabigh city are found in Table 1. The average shear-wave velocity for the topmost 30 m depth, Vs_{30}, ranges from 208.5 m/s to 516 m/s (Fig. 12). The smallest Vs_{30} values (Vs_{30} = 208.5 m/s) are shown in the western zone of the area of interest and increases eastwards, where the highest Vs_{30} values (Vs_{30} = 516 m/s) are found. Furthermore, Vs_{30} values increase due northeastern and southeast zones of the city. The Vs_{30} has the same shape of wadi and basin, where the wadi has lower Vs_{30} values than the adjacent sites. Examples of 1D-Vs profiles through Rabigh city are existing in Fig. 13. The estimated Vs_{30} in Rabigh city was correlated with EC8 standards, as shown in Table 2. Accordingly, the soil profiles in Rabigh city can be characterized into two site soil classes, C and D (Fig. 14). Site soil class C covers the central and the north western zones, while site soil class D is including the western zone of Rabigh city and extends as a strip connecting the northern and southern lagoons.
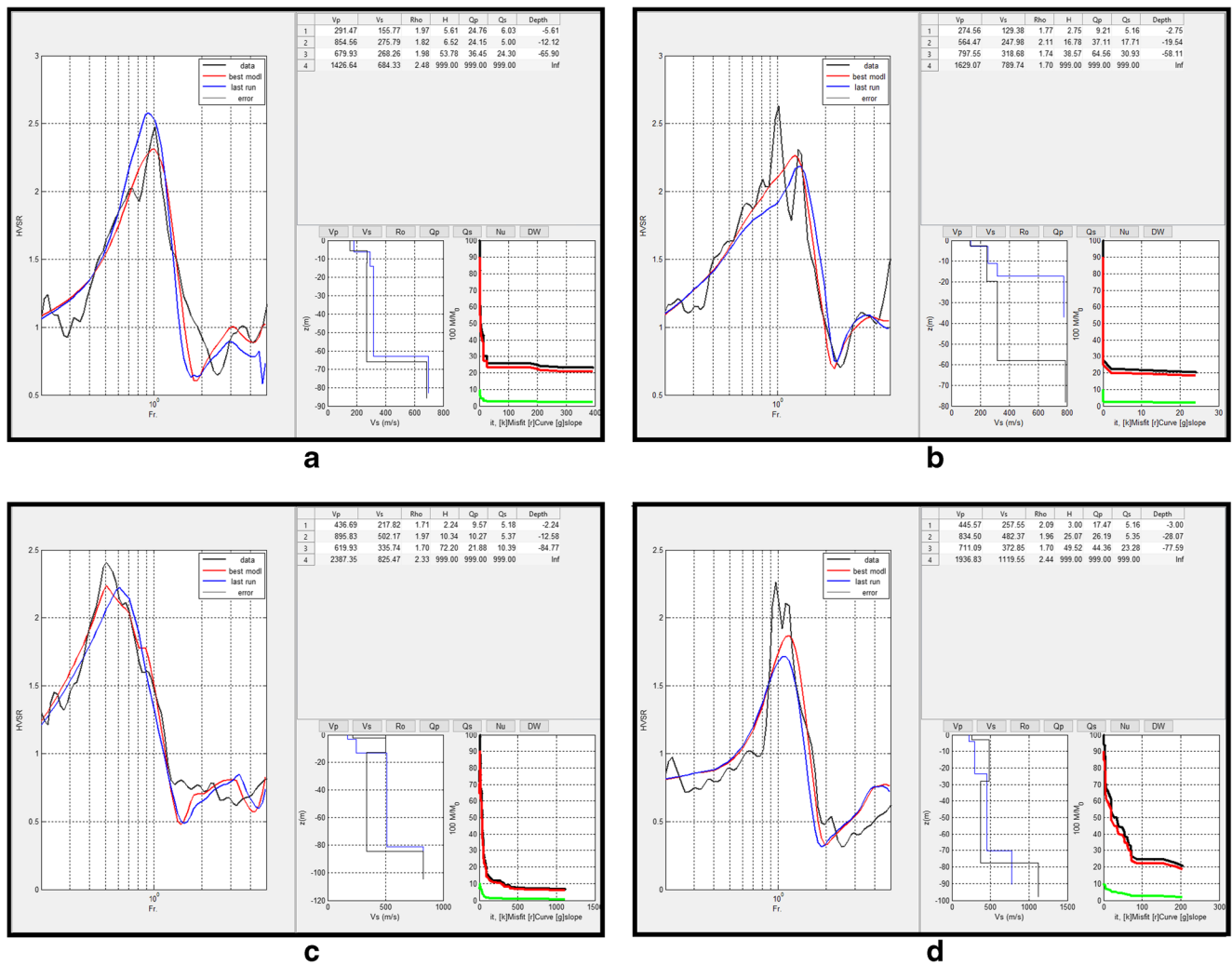
2015; Herak 2008; Lunedei and Albarello 2010; Hassani and Atkinson, 2016; Ahmad and Singh, 2016) including the initial models (P-wave velocity, S-wave velocity, density, thickness, quality of P-wave, and quality of S-wave). An initial soil profile model was obtained for each geological unit by averaging the geotechnical data in each unit. About 87 H/V curves were excluded through the inversion process as they have artificial peaks within the inversion frequency band (0.2 Hz–5 Hz). Finally, 40 of H/V curves covering the study area (Fig. 8) have selected to assess the Vs_{30} profiling in Rabigh city.

a

b

c

d

Fig. 13 Shows HVSR inversion process for (**A**) Qs geologic unit, the left panel is HVSR inversion process, middle panel is 1D Vs output model, and right panel is misfit curve; (**B**) Qal geologic unit, the left panel is HVSR inversion process, middle panel is 1D Vs output model, and right panel is misfit curve, (**C**) Qc geologic unit, the left panel is HVSR inversion process, middle panel is 1D Vs output model, and right panel is misfit curve, (**D**) Qu geologic unit, the left panel is HVSR inversion process, middle panel is 1D Vs output model, and right panel is misfit curve

Discussion and conclusions

Rabigh city is covered by four geological units as distinguished by their differing f_o, A_o, and Vs_{30} values. The unit of alluvial terraces and fans (Qu) has higher values of f_o in the northern than in the southern parts study area, while Vs_{30} increases in the northeastern and southeastern zones. These results can be interpreted to presence of thin and dense soil deposits Qu unit. The unit of alluvial and eluvial gravels and sands (Qal) intersects in the northeastern part, where f_o was

Table 2 Soil classification according to NEHRP (Council 2003)

| Soil type NEHRP	General description	Vs_{30} (m/s)
A	Hard rock	> 1500
B	Rock	$760 < Vs \leq 1500$
C	Very dense soil and soft rock	$360 < Vs \leq 760$
D	Stiff soil $15 \leq N \leq 50$ or 50 kPa $\leq Su \leq 100$ kPa	$180 \leq Vs \leq 360$
E	Soil or any profile with more than 3 m of soft clay defiled as soil with PI >20, w $\geq$ 40%, and Su < 25 kPa	≤ 180
F	Soils requiring site-specific evaluations	
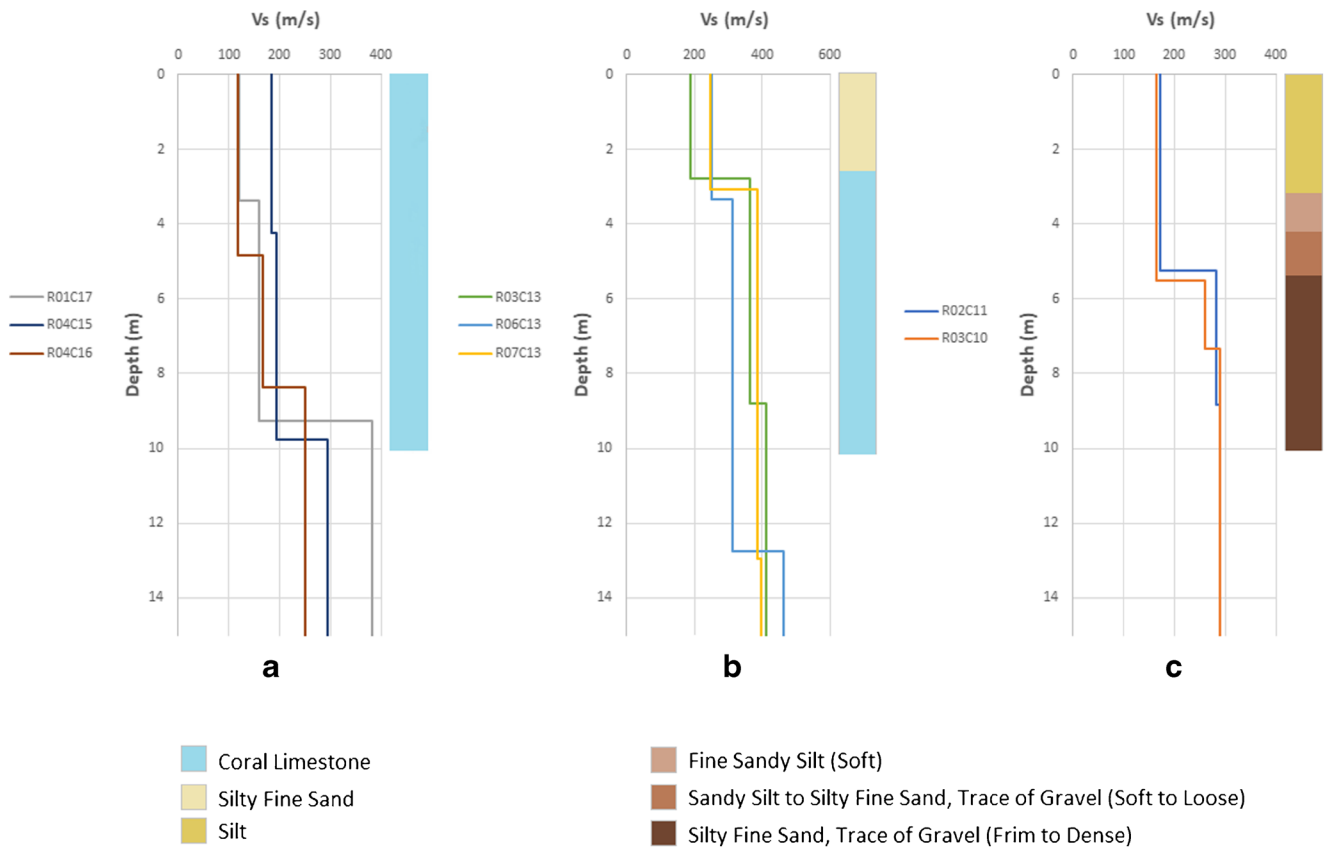
Fig. 14 The correlation between the deduced 1D-Vs$_{30}$ and the geotechnical borehole data in (**A**) coral limestone, (**B**) alluvial and eluvial gravels and sands, and (**C**) sabkhah deposits

lower than the adjacent unit. The A_o and Vs$_{30}$ values increase toward the basin. This means that the sedimentary thickness

increases through the wadi toward the basin, where this basin is covered by a soft soil suggesting a good agricultural farm by

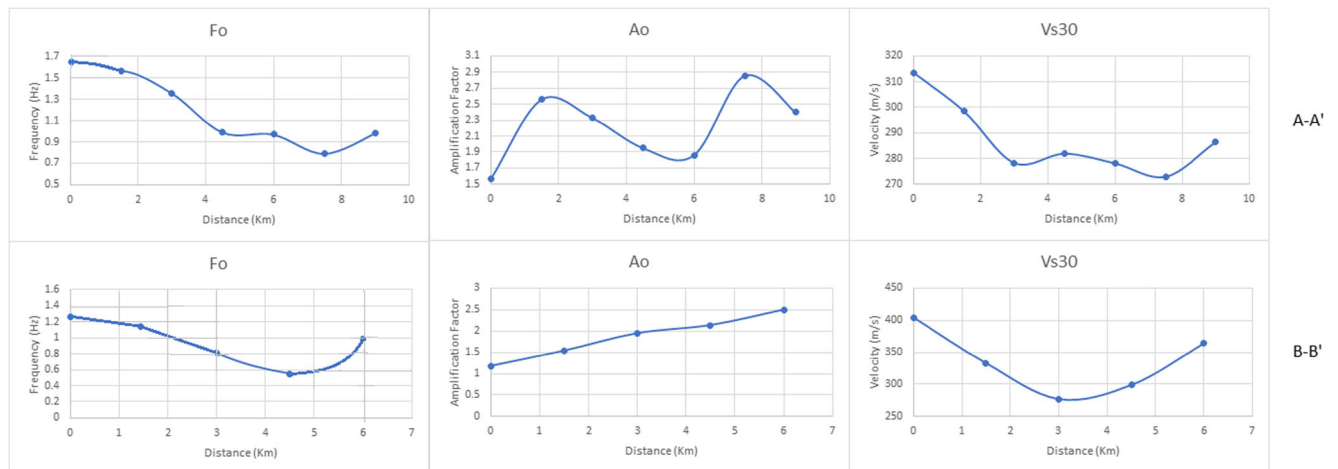**Fig. 15** The selected cross-sections
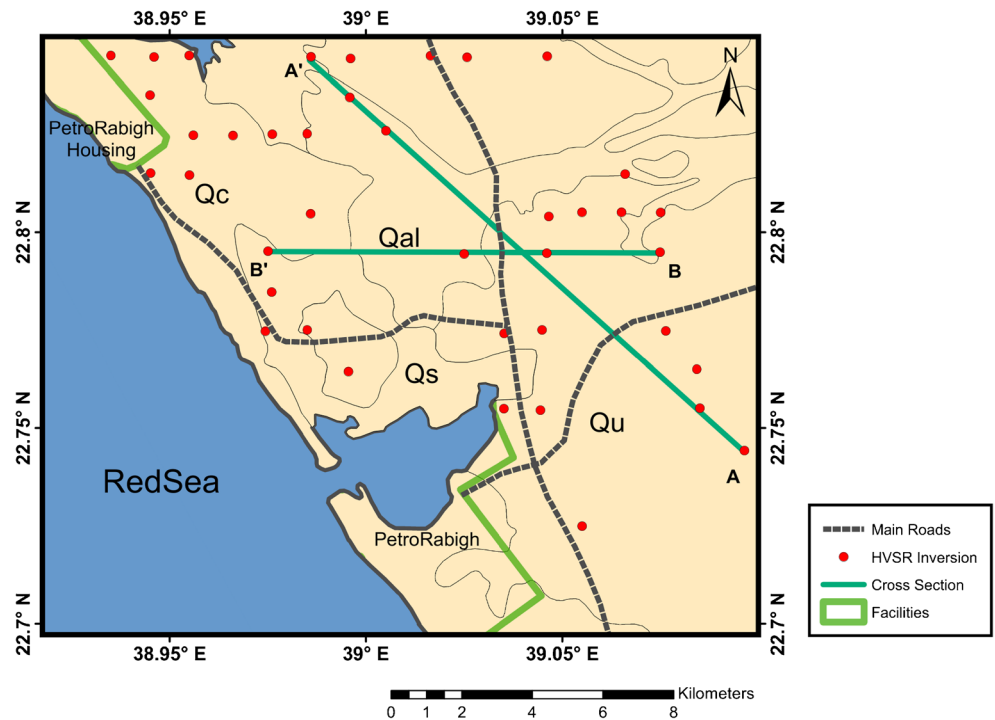
Fig. 16 Two cross-sections A–A′ and B–B′ through the area of study

local citizens. The sabkhah (Qs) unit is splitted into two separate zones; northern zone has moderate f_o and A_o values and low Vs_{30} values. However, the f_o and A_o values of the southern zone decrease and increase toward the coast, respectively, while the Vs_{30} values are high. The reefal limestone (Qc) covers the coastal strip of the city, with moderate f_o and A_o

values which decrease toward the coast. The Vs_{30} values in general decrease due northeastern part. Therefore, Qc can be differentiated as a thick and stiff sediments where thickness increases toward the coastal plain.

The nearest HVSR inversion stations to the geotechnical boreholes show good correlation in Fig. 14. The 1D Vs model
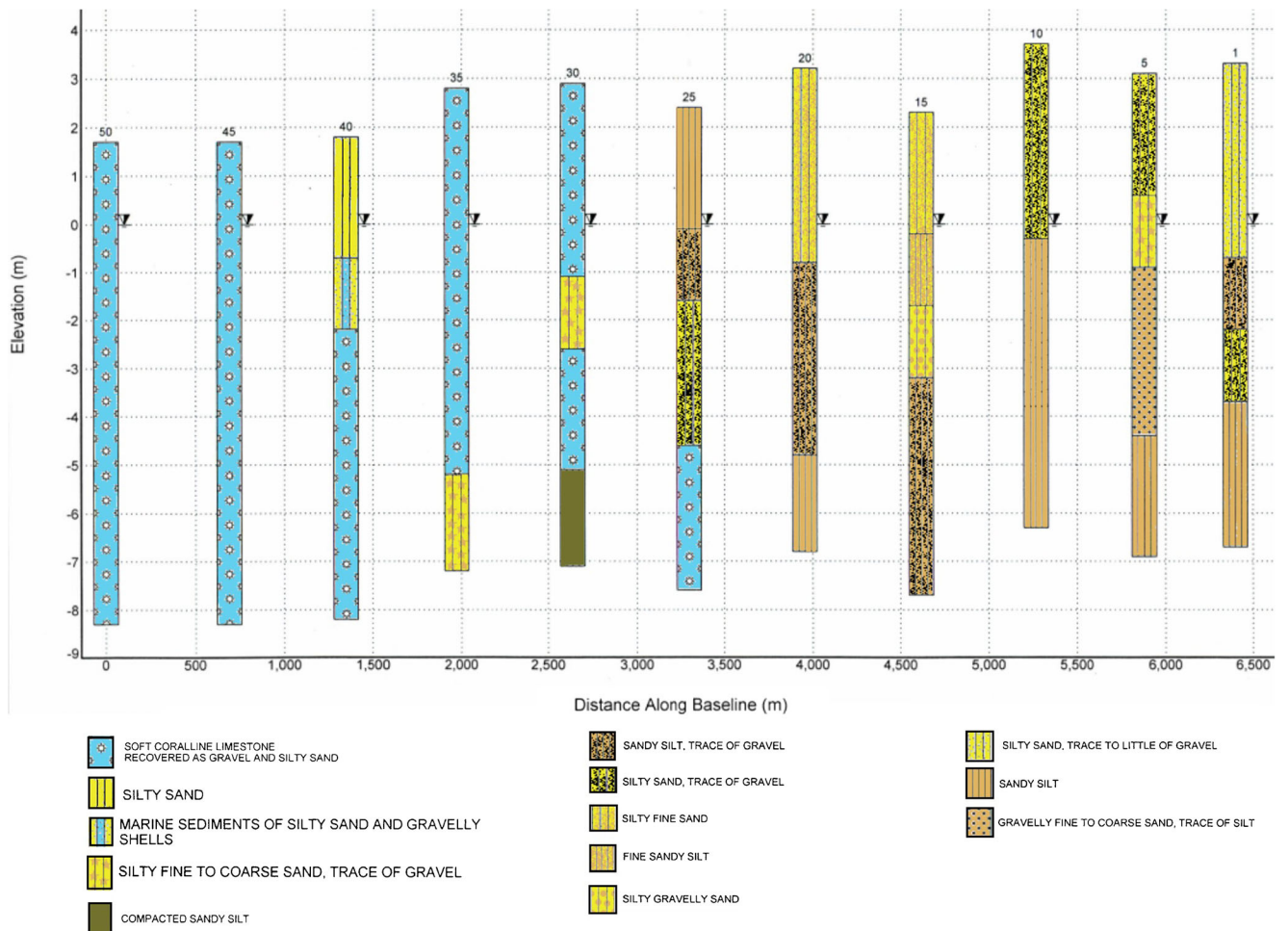

Fig. 17 Subsurface layers' distribution through Rabigh city from geotechnical boreholes (after Adel Engineering Office)

in the coralline limestone (Qc) has low velocity at the three sites, suggesting it is highly weathered limestone due to significant weathering processes. The alluvial and eluvial gravels and sands (Qal) are composed of silty sand varies into sandy silt to silty fine sand in the first layer, while the second layer is consisting of soft to loose and firm to dense sediments, so this layer has the same Vs as the first; the increasing of Vs in the 3rd layer is related to the high density. Geotechnical borehole data of Sabkhah deposits (Qs) are correlated well with the 1D Vs model.

Due to the nature of the coastal area, the topography of the sedimentation surface is variable, which is reflected in the thickness and types of the sediments in the region, which is characterized by rapid change within a short distance. These sediments are laterally changing from west to east where it is noticed that it varies from highly weathered coralline limestone along the coastal strip into sabkhah deposits, into alluvial and eluvial deposits of gravels and sands in the downstream of the main wadi passing through the area and ended by dry and weathered sediments from the mother rocks to the east of the area of study. These rapidly change the thickness, type of sediments, and depth of bedrock level that can be represented in the selected cross-sections A–A′ and B–B′ (Figs. 15, 16). These cross-sections illustrate some sites has no direct and clear relationships between f_0, A_0, and Vs_{30}, where some sites show higher f_0 and higher A_0 and higher Vs_{30} and vice versa, which can be explained in terms of more complicated coastal depositional environments, local structures due to Red Sea floor spreading tectonics, and topography of bedrock level as well.

Figure 17 shows a set of boreholes distributed across the study area. The soft coralline limestone is dominated close to the Red Sea coast, where it has 10 m thickness in boreholes 45 and 50. While in borehole 40, this soft limestone overlain with 2 m thickness of marine silty sand and 2 m of silty sand and then reappears with 8 m thickness in borehole 35, overlying 2 m of silty sand. As moving into land, the coral limestone intercalated with silty sand deposits of 2 m thickness and 2 m of compacted silty sand in boreholes no. 30. This coralline limestone was recorded at depth of 7 m below the ground surface in the borehole 25. As going due east, the silty sand deposits become abundant with more than 10 m depth. Even these sediments vary from silty sand into sandy fine to coarse sand, and sandy silt with traces of gravels.

Based on the abovementioned, it can be concluded that the HVSR inversion technique is a powerful tool to increase the credibility and accuracy of the geotechnical results. In addition, it is highly recommended that detailed field investigations are required to check the characteristics sabkhah deposits covering the northern and southern parts of Rabigh area for seismic risk mitigation especially for the urban zones and great economic projects either existed and/or planned by the Saudi government.

References

Aki K, Richards PG (2002) Quantitative seismology, , 2nd Ed., Published by University Science Books

Aldahri M, Mogren S, Abdelrahman K, Zahran H, El Hady S, El-Hadidy M (2017) Surface soil assessment in the Ubhur area, north of Jeddah, western Saudi Arabia, using a multichannel analysis of surface waves method. J Geol Soc India 89:435–443

Aldahri M, El-Hadidy M, Zahran H, Abdelrahman K (2018) Seismic microzonation of Ubhur district, Jeddah, Saudi Arabia, using H/V spectral ratio. Arab J Geosci 11:113–119. https://doi.org/10.1007/s12517-018-3415-8

Aldamegh KS, Moussa HH, Al-Arifi SN et al (2012) Focal mechanism of Badr earthquake, Saudi Arabia of August 27, 2009. Arab J Geosci 5: 599–606

Almadani S, Al-Amri A, Fnais M et al (2015) Seismic hazard assessment for Yanbu metropolitan area, western Saudi Arabia. Arab J Geosci 8: 9945–9958. https://doi.org/10.1007/s12517-015-1930-4

Ambraseys NN, Melville CP, Adams RD (1994) The seismicity of Egypt, Arabia and the Red Sea, 173 pp. Cambridge University Press, Cambridge

Anbazhagan P, Sitharam TG (2008) Site characterization and site response studies using shear wave velocity. JSEE 10(2):53–67

Arai H, Tokimatsu K (2004) S-wave velocity profiling by inversion of microtremor H/V spectrum. Bull Seismol Soc Am 94:53–63

Bard P-Y (1999) Microtremor measurements: a tool for site effect estimation. The effects of surface geology on seismic motion, Irikura, Kudo, Okada, Sasatani (eds). Melkema, Rotterdam

Bignardi S, Mantovani A, Zeid NA (2016) OpenHVSR: imaging the subsurface 2D/3D elastic properties through multiple HVSR modeling and inversion. Comput Geosci 93:103–113

Council BSS (2003) The 2003 NEHRP recommended provisions for new buildings and other structures, part 1: provisions, FEMA 450/ 2003 edition, 437p

Dawood YH, Aref MA, Mandurah MH (2013) Isotope geochemistry of the Miocene and quaternary carbonate rocks in Rabigh area, Red Sea coast, Saudi Arabia. J Asian Earth Sci 77:151–162

Delgado J, Casado CL, Giner J (2000) Microtremors as a geophysical exploration tool: applications and limitations. Pure Appl Geophys 157:1445–1462

Fäh D, Kind F, Giardini D (2003) Inversion of local S-wave velocity structures from average H/V ratios, and their use for the estimation of site-effects. J Seismol 7:449–467

Farrugia D, Paolucci E, D'Amico S, Galea P (2016) Inversion of surface wave data for subsurface shear wave velocity profiles characterized by a thick buried low-velocity layer. Geophys J Int 206:1221–1231

Hasancebi N, Ulusay R (2007) Empirical correlations between shear wave velocity and penetration resistance for ground shaking assessments. Bull Eng Geol Environ 66:203–213

Hassani B, Atkinson GM (2016) Applicability of the site fundamental frequency as a VS30 proxy for Central and Eastern North America. Bull Seismol Soc Am 106(2). https://doi.org/10.1785/0120150259

Herak M (2008) ModelHVSR—A Matlab® tool to model horizontal-to-vertical spectral ratio of ambient noise. Comput Geosci 34:1514–1526

Konno K, Ohmachi T (1998) Ground-motion characteristics estimated from spectral ratio between horizontal and vertical components of microtremor. Bulletin of the Seismological Society of America, Vol. 88, No. 1, pp. 228-241

Lunedei E, Albarello D (2010) Theoretical HVSR curves from full wavefield modelling of ambient vibrations in a weakly dissipative layered earth. Geophys J Int 181:1093–1108

Lunedei E, Albarello D (2009) On the seismic noise wavefield in a weakly dissipative layered earth. Geophys J Int 177:1001–1014

Mantovani A, Abu Zeid N, Bignardi S, Santarato G (2015) A geophysical transect across the central sector of the Ferrara Arc: passive seismic investigations–Part II. In: GNGTS 2015, 34th national conference. Istituto Nazionale Di Oceanografia E Di Geofisica Sperimentale, pp 114–120. https://doi.org/10.13140/RG.2.1.3213.7687

Mendecki MJ, Bieta B, Mycka M (2014) Determination of the resonance frequency–thickness relation based on the ambient seismic noise records from upper Silesia Coal Basin. Contemp Trends Geosci 3: 41–51

Moore TA, Al-Rehaili MH (1989) Geologic map of the Makkah quadrangle, sheet 21D. Kingdom of Saudi Arabia, Saudi Arabian Directorate General of Mineral Resources Geoscience Map GM-107C, scale 1:

Nakamura Y (1989) A method for dynamic characteristics estimation of subsurface using microtremor on the ground surface. Japanese NationalRailway Technical Research Institute, Quarterly Reports, pp. 25-33

Nakamura Y (1996) Real-time information systems for seismic hazards mitigation UrEDAS, HERAS and PIC. Q Report-Rtri 37:112–127

Nakamura Y (2000) Clear identification of fundamental idea of Nakamura's technique and its applications

Nakamura Y (2009) Basic structure of QTS (HVSR) and examples of applications. Increasing Seismic Safety by Combining Engineering Technologies and Seismological Data 33–51

Parolai S, Picozzi M, Richwalski SM, Milkereit C (2005) Joint inversion of phase velocity dispersion and H/V ratio curves from seismic noise recordings using a genetic algorithm, considering higher modes. Geophysical Research Letters, Vol. 32, L01303, https://doi.org/10.1029/2004GL021115

Ahmad R, Singh RP (2016) Use of remote sensing and topographic slope in evaluating seismic site-conditions in Damascus region. IEEE IGARSS:5777–5780. https://doi.org/10.1109/IGARSS.2016.7730509

Ramsay C (1986) Geologic map of Rabigh quadrangle, sheet 22 D. Ministry of Petroleum and Mineral Resources, Jiddah, Saudi Arabia, Kingdom of Saudi Arabia

Sesame W (2004) Guidelines for the implementation of the H/V spectral ratio technique on ambient vibrations-measurements, processing and interpretation. SESAME European research project, Deliverable D23. 12., Project No. EVG1-CT-2000-00026 SESAME, 62 pp

Tsai NC, Housner GW (1970) Calculation of surface motions of a layered half-space. Bull Seismol Soc Am 60:1625–1651

Wathelet M (2006) Geopsy software manual. Technical Report, SESAME European Project. 251p

Zahran HM, El-Hady SM (2017) Seismic hazard assessment for Harrat Lunayyir–a lava field in western Saudi Arabia. Soil Dyn Earthq Eng 100:428–444

Zahran HM, Sokolov V, Roobol MJ, Stewart ICF, el-Hadidy Youssef S, el-Hadidy M (2016) On the development of a seismic source zonation model for seismic hazard assessment in western Saudi Arabia. J Seismol 20:747–769. https://doi.org/10.1007/s10950-016-9555-y

Zaigham N, Aburizaiza O, Mahar G, Nayyar Z, Al-Amri N (2017) Satellite remote sensing analyses for hydrogeological assessment of Rabigh drainage basin, Red Sea coast, Saudi Arabia. Int J Water Resourc Arid Environ 6(1):1–12

Zor E, Özalaybey S, Karaaslan A et al (2010) Shear wave velocity structure of the Izmit Bay area (Turkey) estimated from active–passive array surface wave and single-station microtremor methods. Geophys J Int 182:1603–1618